



Cite this: *Integr. Biol.*, 2016, 8, 156

## Phenotypic regulation of liver cells in a biofunctionalized three-dimensional hydrogel platform†

Myung Hee Kim,<sup>ab</sup> Supriya K. Kumar,<sup>ab</sup> Hitomi Shirahama,<sup>ab</sup> Jeongeun Seo,<sup>ab</sup> Jae Ho Lee<sup>ab</sup> and Nam-Joon Cho<sup>\*abc</sup>

Loss of function is a major challenge for hepatocytes that are cultured on two-dimensional (2D) cell culture platforms. Biofunctionalized three-dimensional (3D) scaffolds produced by microfabrication strategies can overcome these limitations by presenting vital environmental cues, strong mechanical properties, and three-dimensional geometry to enable high-fidelity liver tissue engineering. Herein, we report the detailed investigation of hepatocarcinoma (Huh 7.5) cellular behavior in a collagen-functionalized microsphere-templated poly(ethylene glycol) (PEG) hydrogel scaffold which promotes 3D hepatic sheet morphology. Collagen conjugation led to improved liver-specific functions, including albumin production and cytochrome P450 (CYP450) activity. Importantly, the gene expression of numerous cell-adhesion markers was enhanced along with stimulated innate hepatocyte fibronectin production. Taken together, the findings reveal a close connection between hepatic cell morphology and gene expression, offering evidence that surface-coated collagen in the 3D hydrogel platform triggers the upregulation of hepatocyte-specific transcription factors and the secretion of liver metabolic markers.

Received 26th October 2015,  
Accepted 28th December 2015

DOI: 10.1039/c5ib00269a

www.rsc.org/ibiology

### Insight, innovation, integration

Curiously, this design prioritizes minimal cell-scaffold interactions, whereas cell-scaffold interactions are a ubiquitous part of liver biology. New material-inspired strategies that induce the formation of cell aggregates with biologically relevant morphologies are of high priority. Here, we report the detailed investigation of hepatocarcinoma (Huh 7.5) cellular behavior in a collagen-functionalized microsphere-templated poly(ethylene glycol) (PEG) hydrogel scaffold which promotes 3D hepatic sheet morphology. Collagen conjugation led to improved liver specific functions, including albumin production and cytochrome P450 (CYP450) activity. Importantly, the gene expression of numerous cell-adhesion markers was enhanced along with stimulated innate hepatocyte fibronectin production. The findings offer evidence that surface-coated collagen in the 3D hydrogel platform triggers the upregulation of hepatocyte-specific transcription factors and the secretion of liver metabolic markers.

## 1. Introduction

The liver is a critical organ, situated as part of the gastrointestinal tract, with an intricate microarchitecture and a broad range of key functions, including detoxification, xenobiotic metabolism, immunologic functions, and production and secretion of a multitude of proteins and bile constituents.<sup>1,2</sup> Liver transplantation is the most effective therapy for patients with acute or chronic

liver diseases and failure, but this therapeutic option is severely hindered by the shortage of liver supply.<sup>3</sup> Alternative treatments being developed include hepatocyte transplantation and extracorporeal bioartificial liver devices, both of which would require proper culturing and maintenance of hepatocyte functions *in vitro*.<sup>2,4</sup>

Given the multifaceted microenvironment of the liver, the culture of hepatocytes on inadequate conventional two-dimensional (2D) substrates has resulted in loss of function and viability of the hepatocytes, especially over an extended period of time.<sup>5–7</sup> The development of three-dimensional (3D) culture platforms and biomatrices for hepatocytes has proven superior and is able to overcome these aforementioned limitations, which are especially useful in the preclinical drug toxicity screening<sup>8</sup> and the development of bioartificial liver support devices.<sup>4</sup>

Current 3D microfabrication strategies and biomaterial constructs aim at mimicking the important aspects of the liver

<sup>a</sup> School of Materials Science and Engineering, Nanyang Technological University, 50 Nanyang Avenue 639798, Singapore. E-mail: njcho@e.ntu.edu.sg; Fax: +65 6790 9081; Tel: +65 6592 7945

<sup>b</sup> Centre for Biomimetic Sensor Science, Nanyang Technological University, 50 Nanyang Avenue 639798, Singapore

<sup>c</sup> School of Chemical and Biomedical Engineering, Nanyang Technological University, 62 Nanyang Avenue 637459, Singapore

† Electronic supplementary information (ESI) available. See DOI: 10.1039/c5ib00269a

microarchitecture. Yarmush and his coworkers studied the viability and function of adult rat hepatocytes in a collagen sandwich culture, an extracellular matrix (ECM) configuration resembling that of the *in vivo* physiology.<sup>9–12</sup> Hepatocytes in the sandwich culture exhibited polygonal morphology in monolayer formation and maintained liver-specific functions. This platform has been enhanced by altering the sandwich material flanking the hepatocyte cord<sup>13</sup> and inducing flow.<sup>8,14,15</sup> Bhatia and her team utilized tunable poly(ethylene glycol) (PEG)-based hydrogels to encapsulate hepatocytes for the study of increased cell–cell interactions in microtissues,<sup>16</sup> biodegradable synthetic hydrogel effect on hepatic functions,<sup>17</sup> and photo- and electro-patterning to control the microenvironment more precisely.<sup>18</sup> Hydrogel-encapsulated co-cultured hepatocytes tend to form interconnected 3D cell networks and had prolonged function. Kotov and colleagues designed a hexagonally packed sphere-templated scaffold to promote 3D cell culture for multiple cell types, especially the formation of spheroids when culturing a hepatocarcinoma cell line (HepG2) in scaffolds made from nonfouling materials.<sup>19–23</sup> These highly ordered, mechanically stable, porous scaffolds promote cell–cell interactions and replenish nutrients and oxygen to the cells while removing secreted waste molecules. While spheroid culture has gained attention, its shortcomings include the presence of necrosis at the aggregates' center,<sup>24</sup> thereby conceding that different cell formation may show better results.<sup>25</sup>

The goal of this study is to examine the synergistic effect of ECM presence and a highly ordered, porous scaffold on hepatocyte behavior. The composition of ECM proteins found in the *in vivo* physiology is specific to each tissue and regulates important cell behavior, such as cell adhesion, by interacting with integrins embedded in the cell membrane.<sup>26</sup> Collagen type I (Col I) is a prevalent ECM protein in the hepatic microenvironment.<sup>27,28</sup> Therefore, we fabricated a Col I-functionalized PEG ICC micro-scaffold and seeded Huh-7.5 cells as our model hepatocyte cell line. The fabrication of the porous bioactive scaffold, ICC topology and the influence of the conjugated collagen concentration on Huh-7.5 cell growth and function were examined in detail.

## 2. Materials and methods

### 2.1 Synthesis of PEG-diacrylate (PEG-DA)

PEG-DA was synthesized according to previously published method without modification.<sup>29,30</sup> Briefly, diol-terminated PEG ( $M_w = 4.6$  kDa; Sigma-Aldrich, MO) was reacted with 2.5 mol excess of acryloyl chloride (Sigma-Aldrich) and triethylamine base catalyst in tetrahydrofuran (THF, Sigma-Aldrich) overnight at room temperature (RT). The resulting PEG-DA was then purified by filtration, liquid–liquid extraction in dichloromethane (Sigma-Aldrich) and precipitation in diethyl ether (Sigma-Aldrich).

### 2.2 PEGDA/PEG-NHS ICC scaffolds

**2.2.1 Fabrication of polystyrene (PS) colloidal crystals (CCs).** An Eppendorf tube (I. D. = 6 mm; Axygen Scientific, NY) glued to a microscopic slide (Bioanalytic GmbH, Germany) was used as the

CC mold. A suspension of PS spheres with a mean diameter of 140  $\mu\text{m}$  ( $139 \pm 2.9$   $\mu\text{m}$ ; Duke Scientific, CA) in 70% ethanol (Merck, Germany) was pipetted into the molds and washed with ethanol (Merck). The assemblies were halfway immersed in an ultrasonic bath (Elma Schmidbauer GmbH, Germany) and sonicated for 2–3 min to arrange the individual spheres into ordered CCs of  $\sim 8$ –13 layers. After complete evaporation of ethanol at RT, the self-assembled CCs were sintered in a furnace at 130  $^{\circ}\text{C}$  for 6 h and removed from the molds.

**2.2.2 Fabrication of PEGDA/PEG-NHS ICC scaffolds.** Hydrogel precursor solution, comprising either 50% (w/v) PEG-DA and 0.05% (w/v) photoinitiator (PI, 2-hydroxy-4'-(hydroxyethoxy)-2-methylpropiophenone; Sigma) or 50% (w/v) PEG-DA, 10% (w/v) acryloyl-PEG-NHS (PEG-NHS; Laysan Bio, AL), and 0.05% (w/v) PI in deionized water, was infiltrated into the CCs by centrifugation. The excess prepolymer solution was removed by blotting. The infiltrated CCs were then exposed to 365 nm UV light ( $10.84$   $\text{mW cm}^{-2}$ ) for 5 min and subsequently soaked in THF for 24 h to dissolve the PS spheres completely. Hydrogel scaffolds with the newly formed ICC pores were immersed in 70% ethanol for 1 h, washed with phosphate buffered saline (PBS; Hyclone, UT; pH 7.4) with centrifugation to remove bubbles and sterilized under UV light for 30 min. Fig. 1A illustrates the schematic of the fabrication of PEG-based hydrogel ICC scaffolds.

**2.2.3 Conjugation of Col I to PEG-NHS ICC scaffolds and visualization.** PEG-NHS scaffolds (scaffolds that contain both PEG-DA and PEG-NHS) were surface-modified by Col I using amine-reactive crosslinker chemistry. Scaffolds were coated with either 20  $\mu\text{g mL}^{-1}$  or 200  $\mu\text{g mL}^{-1}$  solution of Col I from the rat tail (Sigma; diluted in PBS), henceforth denoted Collagen 20 and Collagen 200 ICC scaffolds, respectively, by centrifugation and shaking for 30 min and then incubated at 4  $^{\circ}\text{C}$  overnight.

To visualize the homogeneous coating with collagen, ICC scaffolds were washed twice with PBS after the overnight collagen-conjugation, fixed with 4% paraformaldehyde (PFA; Alfa Aesar, MA) for 5 min, washed again with PBS and incubated with anti-mouse primary antibodies against Col I (1 : 100; Abcam) in 3% BSA overnight at 4  $^{\circ}\text{C}$ . The samples were then washed three times with PBS and incubated with anti-mouse secondary antibodies conjugated with Alexa Flour 488 (1 : 100; Life Technologies) for 2 h. Stained scaffolds were then imaged using a LSM710 confocal microscope and the 3D construction image was created using the ZEN program.

**2.2.4 Surface morphology of ICC scaffolds.** Scanning electron microscopy (SEM) was employed to visualize the ordered cavities formed in the PEG-DA ICC scaffolds. Scaffolds were serially dehydrated in ethanol solution and stored at  $-80$   $^{\circ}\text{C}$  until ethanol evaporated completely. The samples were then dried in a Freezone 4.5 (Lobconco) freeze drier for 48 h, coated with a Pt film of 10 nm thickness using a JFC-1600 (JEOL) sputter coater and the micrographs were acquired using a JSM-7600F (JEOL) FE-SEM instrument at a voltage of 5 kV.

### 2.3 Huh-7.5 cell culture and seeding

Prior to cell seeding, ICC scaffolds were placed in 24-well plates (Corning, NY), washed with PBS, and kept in 2 mL of complete media for 30 min. Media were aspirated and scaffolds were dried

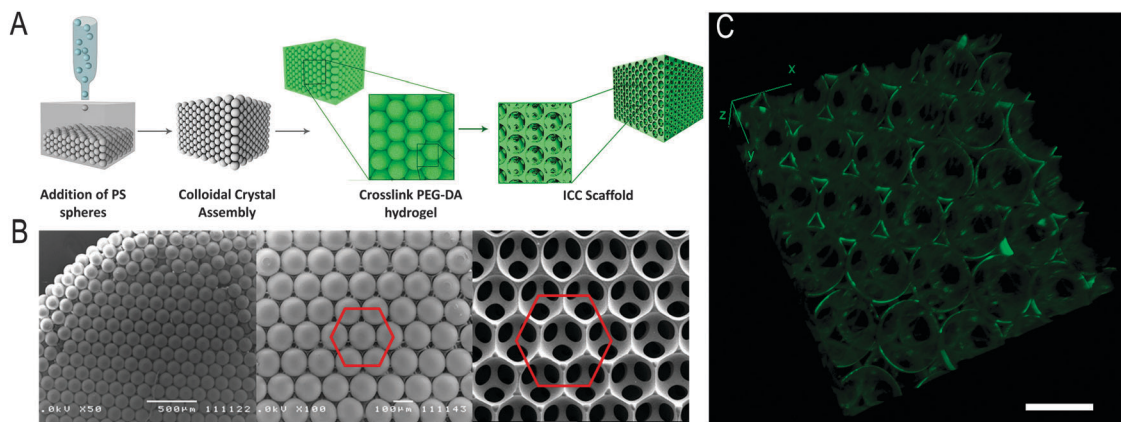


**Fig. 1** PEG-based hydrogel ICC scaffold. (A) Schematic of the ICC scaffold fabrication process. (B) SEM micrographs of self-assembled polystyrene (PS) bead lattices (left, middle; scale bars = 500  $\mu\text{m}$  and 100  $\mu\text{m}$  respectively) and an unseeded, highly ordered PEG-DA ICC scaffold (right; scale bar = 100  $\mu\text{m}$ ). (C) Confocal microscopy 3D image of collagen-conjugated ICC scaffolds (scale bar = 200  $\mu\text{m}$ ). Green indicates the Col I stained by a specific Col I antibody.

for 1 h under UV light for sterilization. Huh-7.5 hepatocarcinoma cells (Apath) were maintained in Dulbecco's modified Eagle's medium (DMEM; Hyclone) supplemented with 10% fetal bovine serum (FBS; Hyclone), 100 U mL<sup>-1</sup> penicillin (Life Technologies, MA) and 100 mg mL<sup>-1</sup> streptomycin (Life Technologies, MA) at 37 °C and 5% CO<sub>2</sub>. One million cells in a 25  $\mu\text{L}$  drop of media ( $4 \times 10^7$  cells per mL) was carefully pipetted on top of each ICC scaffold. After 12 h, cell-laden ICC scaffolds were transferred to new 24-well plates and media was changed every 3 days and maintained at 2 mL.

#### 2.4 Cell-loading efficiency, viability and proliferation

Cell-loading efficiency was evaluated by quantifying the number of cells that adhered to the scaffold. On day 1 post-cell seeding of the Huh-7.5 cells, cell-laden ICC scaffolds were transferred to another 24-well plate. Attached cell viability was analyzed quantitatively using the colorimetric Cell Counting Kit-8 (CCK-8; Dojindo Molecular Technologies, MD) according to the manufacturer's instructions. Concisely, cells were incubated with CCK-8 solution for 1 h at 37 °C and the absorbance values (at  $\lambda = 450$  nm) of the collected media were measured using an Infinite<sup>®</sup> 200 PRO microplate reader (Tecan, Switzerland).<sup>31,32</sup>

Spatial cell viability in ICC scaffolds was qualitatively assessed using the LIVE/DEAD<sup>®</sup> cell viability/cytotoxicity kit (Life Technologies) according to manufacturer's protocol. Briefly, 4  $\mu\text{M}$  calcein-AM and 8  $\mu\text{M}$  ethidium homodimer-1 (EthD-1) were prepared in complete media, added to the cell-laden scaffolds and incubated for 1 h at 37 °C. The stained cells (green: live cells [calcein], red: dead cells [EthD-1]) were visualized using a confocal microscope (LSM710, Carl Zeiss).

Cell proliferation was assessed using the CCK-8 assay on days 1, 4, 7, 10 and 14 and normalizing the measured absorbance values to day 1 values for each condition. For later albumin secretion normalization, raw absorbance values were also converted to cell number using a standard curve.

#### 2.5 Cell function and immunohistochemical staining

The amount of albumin secreted in media, collected every 3 days and stored at -80 °C until use, was detected and quantified

using a human albumin enzyme-linked immunosorbent assay (ELISA) kit (Abcam, UK). ELISA was performed according to manufacturer's instructions. Data were normalized against the cell number and the amount of albumin on day 1.

For immunohistochemical analysis, albumin and CYP3A4 were stained to spatially visualize the cell function of the hepatocytes in the 3D scaffolds on specific days. Huh-7.5-ICC scaffold constructs were washed twice with PBS, fixed with 4% PFA for 5 min, permeabilized with 0.1% Triton X-100 (Bio-Rad, CA) in PBS for 30 min, washed again with PBS and incubated in 3% BSA blocking buffer in PBS for 1 h. Cells were then incubated with anti-mouse primary antibodies against CYP3A4 or albumin (1 : 100; Santa Cruz Biotechnology, CA) overnight at 4 °C and then washed three times with PBS to remove unbound primary antibodies. The cells were incubated with anti-mouse secondary antibodies conjugated with Alexa Flour 488 (1 : 100; Life Technologies). At the same time, filamentous actin (F-actin) was stained with Alexa Flour 555 labelled phalloidin (Life Technologies) for 2 h at RT. After washing twice with PBS, cells in the ICC constructs were counterstained with 10  $\mu\text{g mL}^{-1}$  2,6-diamidino-2-phenylindole dihydrochloride (DAPI; Life Technologies) for 5 min and immediately imaged using a confocal microscope.

#### 2.6 RNA extraction, reverse transcription and quantitative real time PCR

Isolation of total RNA, synthesis of cDNA, and quantitative real-time PCR were carried out as described previously.<sup>33</sup> To isolate RNA, the cell-laden ICC scaffolds were homogenized with TRIzol reagent (Life Technologies) and RNA concentration was measured using Nanodrop (ThermoFisher Scientific; DE, USA). RNA was converted to cDNA through the synthesis of the first strand cDNA using iScript Reverse Transcription Supermix (Bio-Rad Laboratories, CA). Next, SYBR green-based real-time quantitative PCR (qPCR) was performed with the SYBR select Master Mix for CFX (Life Technology) in the CFX connect Real-Time PCR system using amplification mode (95 °C for 20 s, followed by 40 cycles of 10 s at 95 °C, and 40 s at 60 °C). The following genes

Table 1 Primer sequences used in real-time PCR

Target gene	Forward (5′–3′)	Reverse (5′–3′)
<i>Albumin</i>	CTGCACAGAATCCTTGGTGA	CTCCTTATCGTCAGCCTTGC
<i>AAT</i>	GATGCTGCCAGAAAGACAGA	GGAGTTCCTGGAAGCCTTCA
<i>G6P</i>	TTCCTGTTTCAGCTTCGCCAT	TCAAAGACGTGCAGGAGGAC
<i>TAT</i>	GAGTCAGCGCATTGTTGGGAC	ACTAACCGCTCCGTGAACCT
<i>CYP3A4</i>	ACCGTGACCCAAAGTACTGG	TTCAGGGGGATCTGTGTTTC
<i>CYP3A7</i>	AAGTGGACCCAGAACTGCA	GGCTCCACTTACGGTCTCAT
<i>HNF4<math>\alpha</math></i>	TCGTTGAGTGGGCCAAGTAC	TGTCATCGATCTGCAGCTCC
<i>HNF6</i>	TTGAGCCATTGAGCGGACAT	GGCAGGTTCAAACGTTAGGG
<i>Integrin <math>\beta</math></i>	GAAGGGCGTGTGGTAGACA	GTTGCACTCACACACACGAC
<i>E-Cadherin</i>	AGGCCAAGCAGCAGTACATT	AAATGTGTCTGGCTCCTGGG
<i>N-Cadherin</i>	CCTTTCAAACACAGCCACGG	TGTTTTGGGTCCGGTCTGGATG
<i>hepaCAM</i>	ATTTTCGAGGCCACAGGTGTT	TCTCCACCATGCAGCTGTAC
<i>GAPDH</i>	CCATGGGGAAGGTGAAGGTC	CTCGCTCTGGAAGATGGTG

were evaluated: (1) albumin; (2) alpha-1-antitrypsin (AAT); (3) glucose-6-phosphatase (G6P); (4) tyrosine aminotransferase (TAT); (5) cytochrome P450 3A4 (CYP3A4); (6) cytochrome P450 3A7 (CYP3A7); (7) hepatocyte nuclear factor 4-alpha (HNF4 $\alpha$ ); (8) hepatocyte nuclear factor 6-alpha (HNF6 $\alpha$ ); (9) integrin beta-1 (Integrin  $\beta$ 1); (10) E-cadherin; (11) N-cadherin; (12) hepatocyte cell adhesion molecule (hepaCAM); and (13) glyceraldehyde-3-phosphate dehydrogenase (GAPDH). Data were analyzed by the  $2^{-\Delta\Delta CT}$  method, as described previously.<sup>34</sup> The detected levels of each gene mRNA were normalized against GAPDH. Primers were chosen with an online primer design program<sup>35</sup> and listed in Table 1.

### 2.7 Statistics

The statistical significance of differences between the groups was determined using paired two-tailed Student's *t*-test. Significance of gene expression was determined using GAPDH-normalized  $2^{-\Delta\Delta CT}$  values. All data are represented as mean  $\pm$  SD. \*,  $p < 0.05$ ; \*\*,  $p < 0.01$ ; \*\*\*,  $p < 0.001$ .

## 3. Results

### 3.1 Huh-7.5 cell seeding in the highly ordered PEG-DA scaffolds with Col I-coating

PEG-based hydrogel ICC scaffolds were successfully fabricated using a self-assembled polystyrene (PS) colloidal crystal (CC) template. SEM micrographs show the packed hexagonal bead lattice, constructed from the PS spheres 140  $\mu$ m in diameter, and the highly ordered and distinct pore cavities formed after PEG-DA hydrogel polymerization and particle leaching (Fig. 1B). The sphere size used and the annealing time resulted in a mean pore and cavity interconnection diameter of 102  $\mu$ m and 39  $\mu$ m respectively, after dehydration of the scaffold. This porogen diameter was specifically chosen to limit the size and promote the function of the hepatocyte spheroids,<sup>21</sup> known to form in nonadhesive ICC scaffolds, thereby allowing proper penetration of nutrients and oxygen into all Huh-7.5 cells. The 3D confocal image shows uniform conjugation of collagen along the surface of the porous scaffold (Fig. 1C).

After cell seeding, the Huh-7.5 cells were able to infiltrate the ICC scaffolds, settling into the cavities. The cell loading efficiency was evaluated in the PEG-DA scaffolds, with and without Col I conjugation, with an initial cell density of  $1 \times 10^6$  cells per well (Fig. 2A). The seeding efficiency was significantly greater for the PEG-NHS ICC scaffolds and those coated with Col I in comparison to the bare PEG-DA scaffolds. The increased number of unattached cells in the bio-inert PEG-DA scaffold suggests both the Col I coating and the presence of a NHS ester promote cell adhesion.

### 3.2 Viability and proliferation of Huh-7.5 in Col-1 functionalized PEG-DA scaffolds

To understand the effect of ECM presence on Huh-7.5 growth within the ICC scaffolds, the cell proliferation, viability and organization were evaluated. Proliferation of the seeded Huh-7.5 cells, measured quantitatively using a colorimetric cell counting kit, was shown to notably increase in 3D scaffolds compared to the attenuated growth of cells on a 2D plastic culture plate (Fig. 2B). Among the 3D scaffolds, cells in the 200  $\mu$ g mL<sup>-1</sup> Col I coating demonstrated the steadiest proliferation through all 14 days of culture, whereas the other three scaffolds showed a slight reduction on day 14. By day 14, this propagation value was approximately 2.5-fold higher than that of the 2D culture on day 14.

Live/dead staining and confocal imaging showed that Huh-7.5 cells were highly viable in all scaffolds but showed marked differences in growth patterns (Fig. 3). In accordance with previous reports,<sup>21–23</sup> the Huh-7.5 cells formed spheroids in the bare PEG-DA scaffolds and increased in diameter with progression of time. Strikingly, the presence of the Col I coating directed the cells to line the cavity walls and these cell sheets then thickened and the cell–cell interaction between cavities was visibly seen as early as day 1. Interestingly, the PEG-NHS scaffolds initially promoted cell adhesion to the pore surface, most likely through the NHS ester–primary protein interaction, which supported the high seeding efficiency observed in Fig. 2A. However, this interaction was not strong enough and by day 14, the cells start to detach slightly from the walls, and migrate to the center.

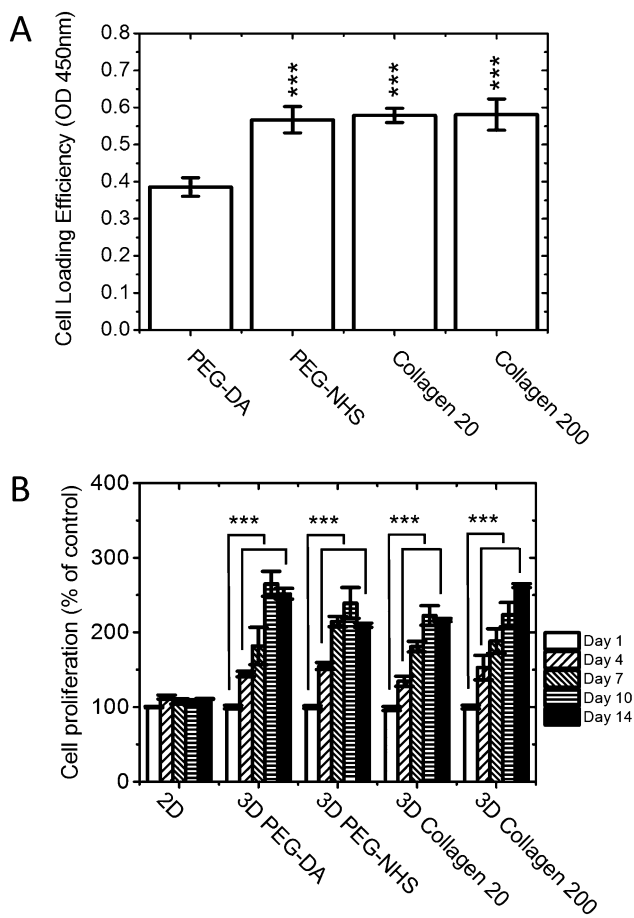


**Fig. 2** Effect of collagen conjugation and scaffold dimension on Huh-7.5 cell loading efficiency and proliferation. Huh-7.5 cells were seeded in 2D and/or 3D ICC scaffolds with or without conjugated Col I. (A) Cell loading efficiency was determined by the CCK-8 colorimetric assay spectrophotometer absorbance measurements on cells within the 3D ICC scaffolds 24 h post-cell seeding. (B) Cell proliferation was quantified by CCK-8 assay on 1, 4, 7, 10, and 14 days post-cell seeding. The data were normalized to day 1 absorbance values (Fig. 2A). ( $n = 3$ , mean  $\pm$  SD. \*:  $p < 0.05$ . \*\*:  $p < 0.01$ . \*\*\*:  $p < 0.001$  compared to CCK-8 absorbance reading for (A) PEG-DA group or (B) day 1 of each group).

### 3.3 Evaluation of Huh-7.5 albumin secretion and CYP3A4 activity in Col-1 functionalized PEG-DA scaffolds

Given the distinct Huh-7.5 growth patterns in PEG-DA ICC scaffolds with and without bioactive surface modification, metabolic activities specific to the liver were then assessed. During the first four days, the albumin secretion rates significantly increased in PEG-NHS and both collagen coated 3D ICC scaffolds (Fig. 4). With prolonged culture, albumin secretion in the bare PEG-DA and PEG-NHS scaffolds faltered while there was a parallel relationship between the Col I conjugated concentration and the albumin production rate. The ICC scaffold conjugated with  $200 \mu\text{g mL}^{-1}$  Col I displayed an albumin secretion rate approximately 1.5 times higher than the PEG-NHS ICC scaffold with and without  $20 \mu\text{g mL}^{-1}$  conjugated Col I and 4 times higher than the bare ICC scaffold. Further characterization of the Huh-7.5 cell behavior by immunohistochemical staining confirmed

the morphological formation of the cells and revealed the spatial visualization of intracellular albumin (Fig. 5A) and CYP3A4 activity (Fig. 5B). Importantly, cell staining showed a high concentration of albumin and CYP3A4 activity in Huh-7.5 cells in collagen coated ICC scaffolds near the interconnections of the cavities, suggesting a dependence on the cell-cell interaction. Confocal images near the top of the scaffold showed a more even distribution of the plasma protein secretion and metabolic enzyme, but a higher activity again in the Col I conjugated ICC scaffolds (Fig. 2A and B, ESI†).

### 3.4 Hepatocyte-specific gene expression in Col I-functionalized PEG-DA scaffolds

In addition to a direct evaluation of the hepatocyte phenotype, the effect of collagen conjugation on hepatocyte-specific gene expression was also quantified by RT-qPCR after total RNA extraction. The mRNA levels for AAT, and G6P, HNF6 and CYP3A4 were significantly up-regulated in a time-dependent manner while cultured in all ICC scaffolds, independent of the surface modification (Fig. 6A, B, D and E). However, other hepatocyte-specific genes, albumin and TAT, were markedly up-regulated in a dose-dependent manner of Col I on ICC ( $p < 0.05$ , Fig. 6G and H). The highest induction in transcription factors such as HNF4 $\alpha$  and HNF6, which regulate the expression of liver secretory proteins,<sup>36</sup> such as albumin,<sup>37</sup> AAT,<sup>38</sup> TAT<sup>39</sup> and G6P,<sup>40</sup> was observed when multilayer cell sheets formed in the presence of  $200 \mu\text{g mL}^{-1}$  collagen after 14 days (Fig. 6C and D). Similarly, CYP3A4 and CYP3A7, members of the cytochrome P450 subfamily involved in Phase I xenobiotic metabolism,<sup>41,42</sup> displayed the highest mRNA expression in the high dose Col I-conjugated ICC group (Fig. 6E and F).

In addition, as shown in Fig. 3, cell adhesion to the scaffold was significantly increased in collagen coated ICC scaffolds in comparison to the bare PEG-DA ICCs, suggesting that the presence of collagen promoted cell adhesion. To obtain more detailed molecular information about the transcriptional level of genes responsible for the improved cell adhesion, the expression of hepatocyte adhesion marker genes E- and N-cadherin,<sup>43</sup> hepaCAM<sup>44</sup> and integrin  $\beta$ 1 was analyzed (Fig. 6I-L). Huh-7.5 cells, which formed multilayer cell sheets in Col I-conjugated ICCs, exhibited an up-regulation of the four aforementioned hepatocyte-specific adhesion transcripts, especially E-cadherin and hepaCAM. In 2005, Moh *et al.* reported that hepaCAM is expressed in all normal and non-tumorous liver tissues and these molecules can mediate the accelerated cell-matrix adhesion.<sup>44</sup> These data indicate that collagen markedly enhanced cell attachment by up-regulation of E-cadherin and hepaCAM in the 3D ICC platform.

### 3.5 Secretion of ECM by Huh-7.5 in Col I-functionalized PEG-DA scaffolds

Lastly, to determine whether the presence of Col I on scaffolds affected the innate ability of hepatocytes to remodel their surrounding ECM, Col I and fibronectin mRNA levels were quantified. The mRNA transcript levels indicate that fibronectin was up-regulated in a time dependent manner and

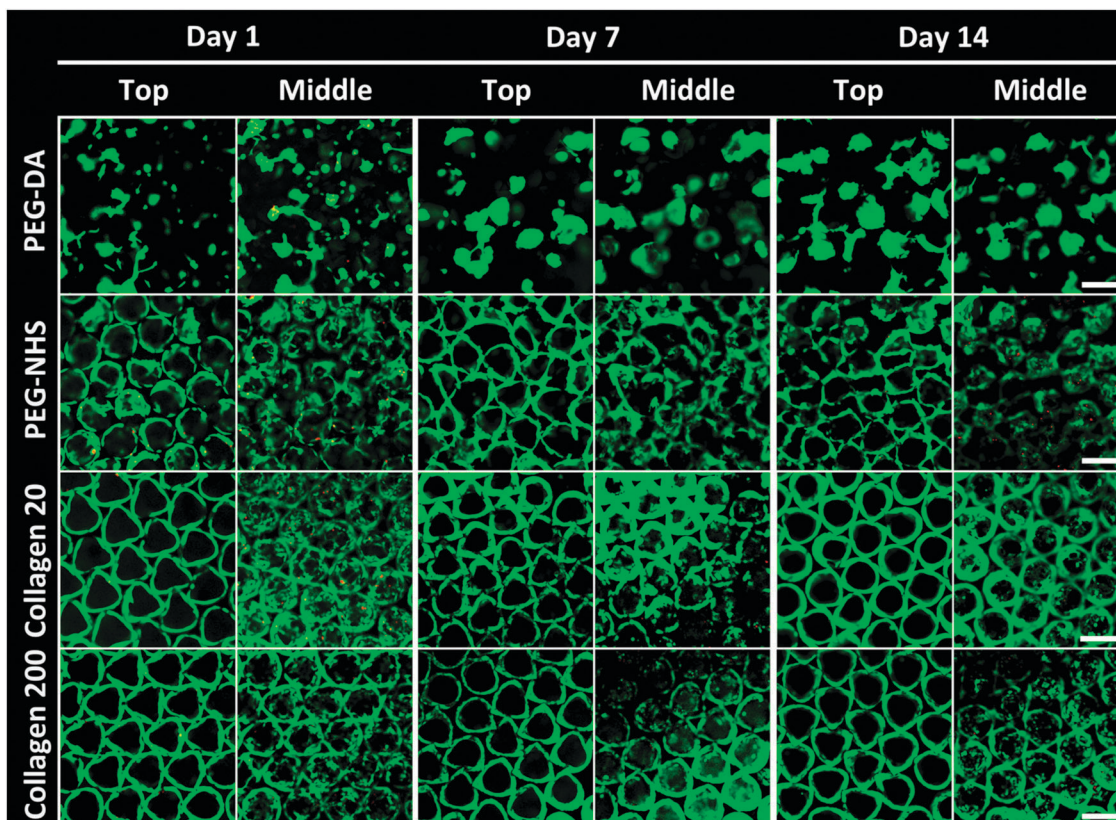


Fig. 3 Evaluation of Huh-7.5 cell viability and growing pattern in 3D ICC scaffolds with and without conjugated Col I. Representative confocal z-stack images of Huh-7.5 cells after live/dead staining taken near the top plane ( $z = 0\text{--}2\ \mu\text{m}$ ) and the middle plane ( $z = -30\ \mu\text{m}$ ) of an ICC scaffold spherical cavity (scale bars =  $200\ \mu\text{m}$ ; image positions are further explained in the ESI† Fig. S1). Green indicates live cells and red indicates dead cells.

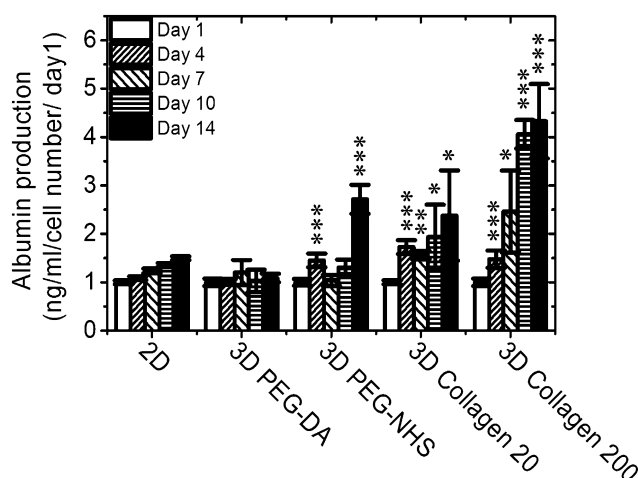


Fig. 4 Evaluation of Huh-7.5 cell albumin secretion in 2D and/or 3D ICC scaffolds with or without conjugated Col I. Albumin secretion was measured from media samples collected on days 1, 4, 7, 10 and 14 by albumin ELISA for liver specific function. The data were normalized by the cell number according to the metabolic rate (refer to Fig. 2B) and day 1 values. ( $n = 3$ , mean  $\pm$  SD; \*:  $p < 0.05$ ; \*\*:  $p < 0.01$ ; \*\*\*:  $p < 0.001$  compared to albumin production on day 1 of each group).

the highest expression was in the  $200\ \mu\text{g mL}^{-1}$  Col-I coated scaffolds (Fig. 7). There is no apparent trend for the Col I profile

based on the varied concentration of conjugated Col-I. However, the increase in Col-I expression in  $200\ \mu\text{g mL}^{-1}$  Col-I conjugated scaffolds is significant on day 14.

## 4. Discussion

One of the main challenges posed in liver tissue engineering is the design of an *in vitro* platform that will be able to maintain primary hepatocyte function over an extended period of time. The difficulty lies in the complexity of the native tissue architecture and the delicacy of the primary hepatocytes. The problem of acquiring and keeping primary hepatocytes has been temporarily bypassed by using model cells—inexpensive immortalized or carcinoma cell lines—that retain most of the hepatic functions with a few differences.<sup>45</sup> Great efforts and strides have been made to try and recreate the intricacies of the liver microarchitecture by combining various aspects of the hepatic microenvironment—ECM-presence, co-culture, mechanical properties, geometry, chemical gradients and flow. Spheroid culture has been a promising technology, focusing on the scaffold geometry, because of the high diffusion properties and cell-cell interactions. However, given that the limitation is the oxygen and nutrient penetration depth, the aggregation of cells above a diameter of  $150\text{--}200\ \mu\text{m}$ <sup>46</sup> results in necrosis of cells present in the center. In the present study, we developed a biofunctionalized

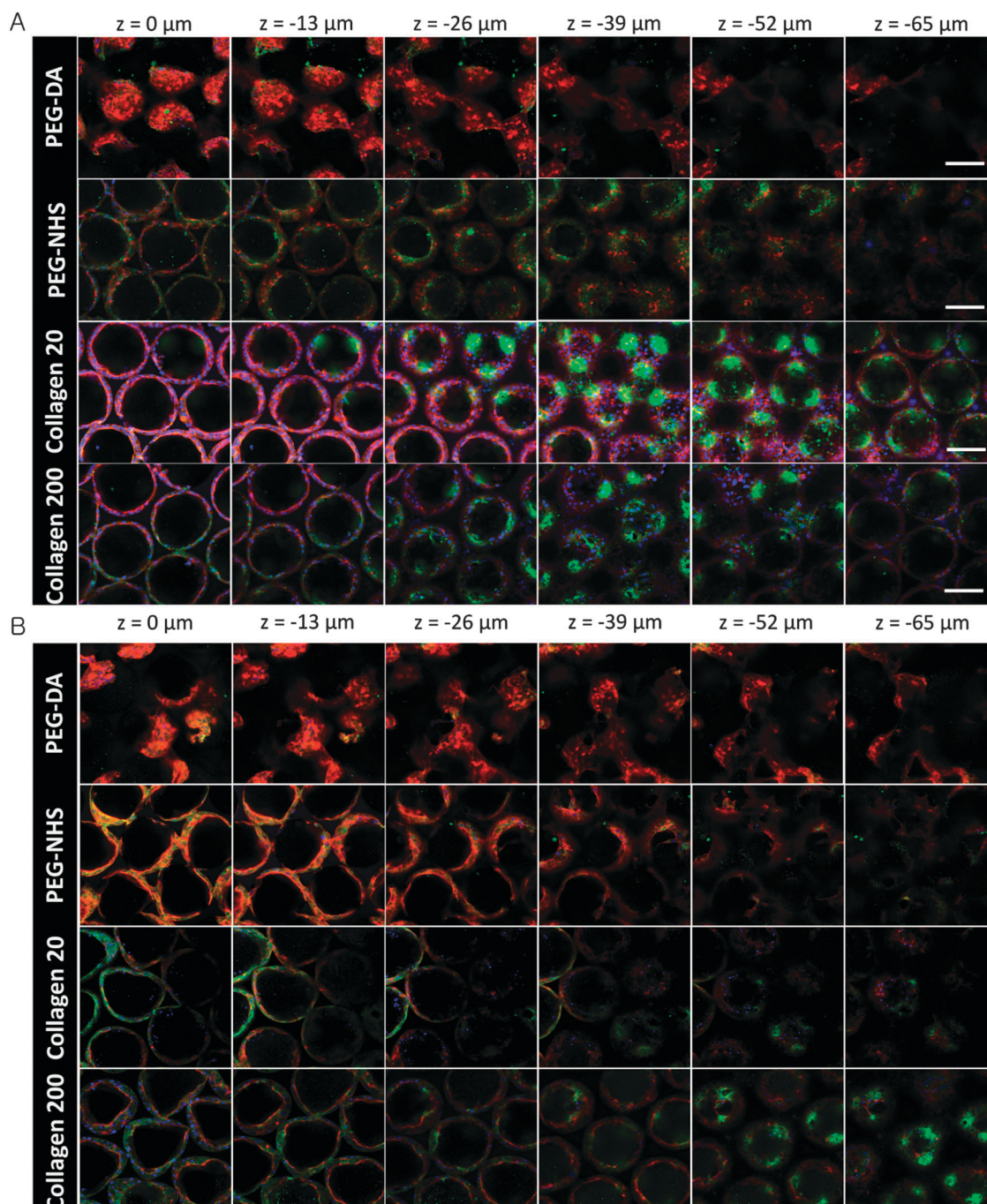
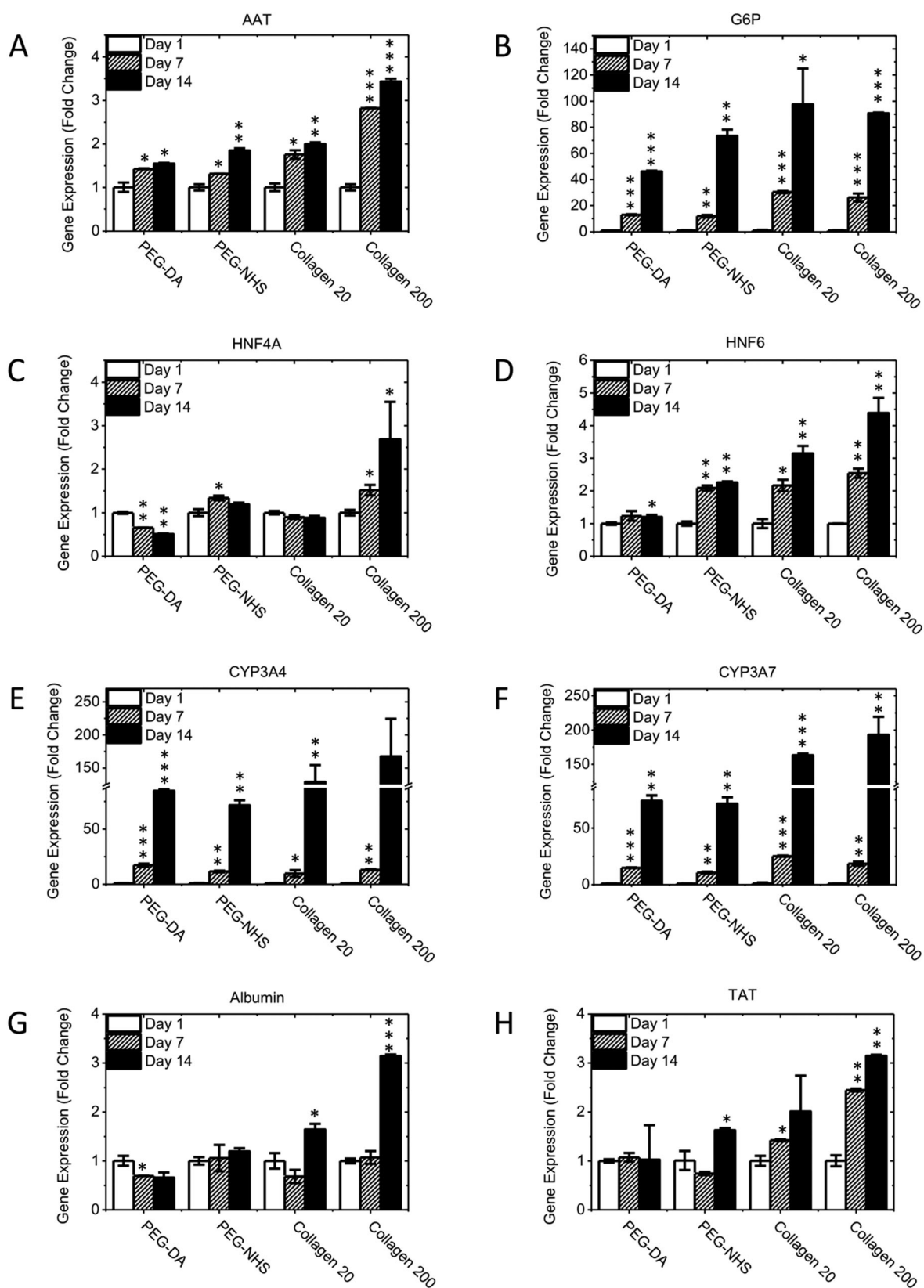


**Fig. 5** Evaluation of spatial liver specific function of Huh-7.5 cells by immunohistochemistry. Huh-7.5 cells were seeded in Col I coated or bare 3D ICC scaffolds and stained for F-actin (red), counterstained by DAPI for DNA (blue), and stained for either (A) albumin (green) on day 7 or (B) CYP3A4 (green) on day 14. Representative confocal z-stack images show stained Huh-7.5 cells from the top ( $z = 0 \mu\text{m}$ ) to the interconnecting channel ( $z = -65 \mu\text{m}$ ) of the ICC scaffold spherical cavity in a serial manner (scale bars =  $100 \mu\text{m}$ ).

PEG hydrogel scaffold that combines geometry and collagen presence to direct the hepatocarcinoma cells into sheet morphology and enhance liver-specific functions.

The fabrication process, using PS spheres, yielded immaculately uniform interconnected cavities displaying the desired hexagonal structure (Fig. 1). Given the cavity size was approximately  $102.3 \mu\text{m}$  (measured from the dehydrated SEM image of the scaffold),

the hepatocyte spheroid in the base 3D PEG-DA scaffold had a diameter smaller than the critical value for necrosis and showed similar proliferation rates in comparison to the hepatocyte multi-sheet formation in collagen-conjugated scaffolds (Fig. 2). Interestingly, PEG-NHS scaffolds, without Col I conjugation, displayed signs of cell adhesion similar to that observed in collagen-conjugated scaffolds (Fig. 3). NHS esters have been



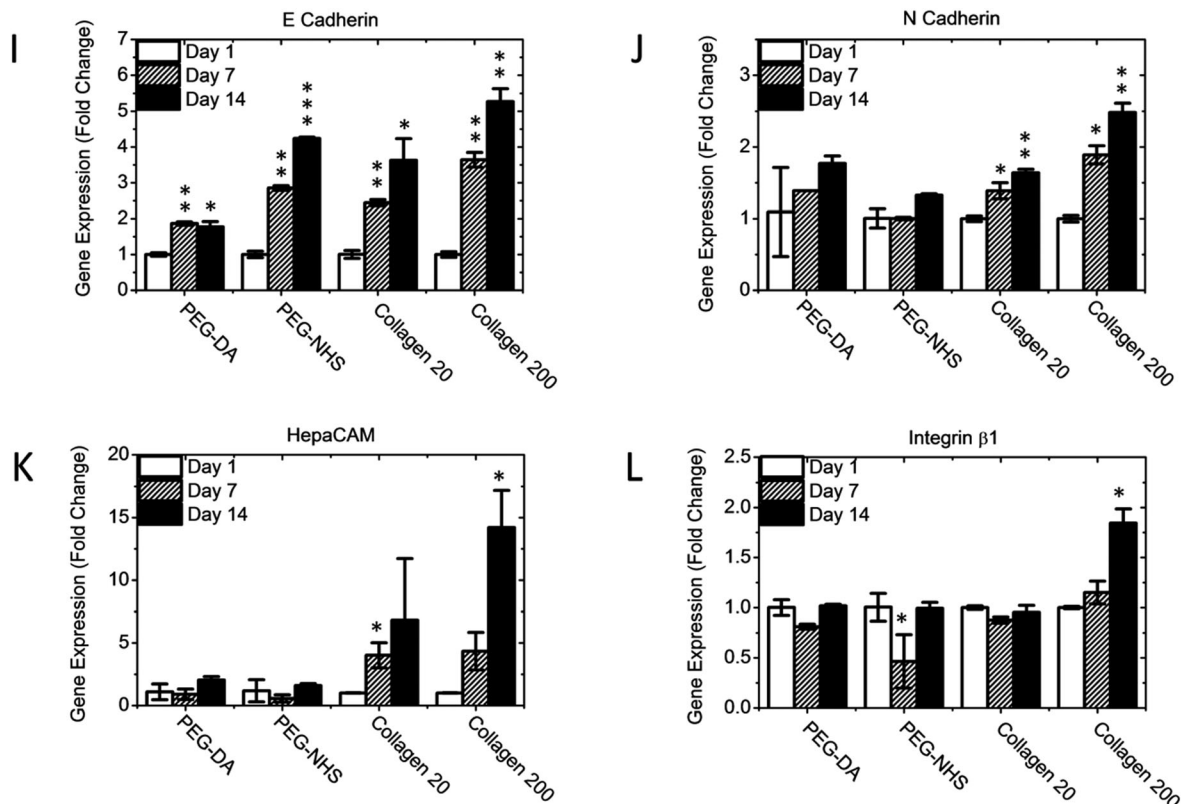


Fig. 6 Effect of collagen conjugation on liver specific gene expression. Huh 7.5 cells were cultured in 3D ICC scaffolds with or without conjugated Col I, and RNA was extracted for the quantitative real-time PCR analysis of (A) alpha-1-antitrypsin (AAT), (B) glucose-6-phosphatase (G6P), (C and D) hepatocyte nuclear factors, (E and F) enzymes in the CYP3A subfamily of the CYP450 family (G) albumin, (H) tyrosine aminotransferase (TAT), and (I–L) cell adhesion proteins. The mRNA expression levels were normalized by GAPDH. ( $n = 3$ , mean  $\pm$  SD; \*:  $p < 0.05$ ; \*\*:  $p < 0.01$ ; \*\*\*:  $p < 0.001$  compared to gene expression on day 1 of each group).

shown to interact with the Lys residue that is prevalent on many proteins, including cell membrane proteins.<sup>47</sup> However after 7 days, the cells start to drift towards the center and aggregate there. Thus, the importance of cell adhesion strength in maintaining morphology integrity is to be noted. The distinct cell growth pattern—multilayer cell sheet—in collagen-conjugated

scaffolds could give rise to unique properties of the cultured cells *versus* spheroids in PEG-DA scaffolds.<sup>48</sup>

Despite similar proliferation rates, the collagen-coated scaffolds displayed higher albumin secretion in a dose-dependent manner, highlighting the functional importance of cell–cell interactions and cell–ECM interactions. Importantly, the stark

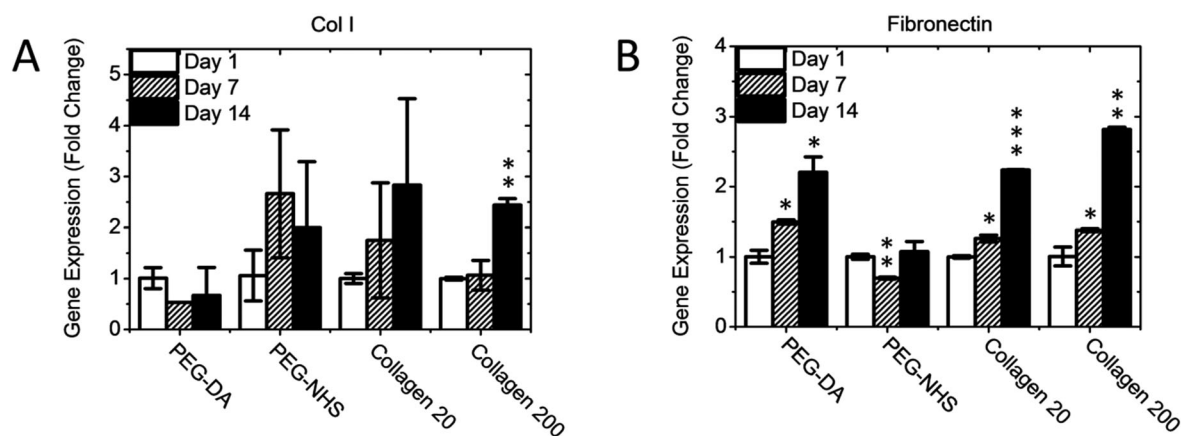


Fig. 7 Effect of collagen conjugation on ECM gene expression. Huh 7.5 cells were cultured in 3D ICC scaffolds with or without conjugated Col I, and RNA was extracted for the quantitative real-time PCR analysis of (A) Col I and (B) fibronectin. The mRNA expression levels were normalized by GAPDH. ( $n = 3$ , mean  $\pm$  SD; \*:  $p < 0.05$ ; \*\*:  $p < 0.01$ ; \*\*\*:  $p < 0.001$  compared to gene expression on day 1 of each group).

difference in the formation of cell morphology led to differences in gene expression regulation. In conjunction with other liver-specific genes described in the results, Touboul *et al.* reported that TAT is also considered to be a marker of mature hepatocytes.<sup>39</sup> Also, Fu and colleagues demonstrated that TAT is a novel tumor suppressor gene and its inactivation, caused by gene deletion and hypermethylation, contributes to the pathogenesis of hepatocellular carcinoma and this enzyme has the highest activity in the liver.<sup>49</sup> In this study, our results suggest that collagen potentially acts as a stimulator in 3D ICC by up-regulation of hepatocyte specific transcription factors (HNF6) and secretion of liver metabolic markers (especially TAT and AAT), when compared to culture in bare scaffolds.

In the broader context of ECM–cell interactions, it remains to be investigated whether other ECM proteins also promote liver-specific functions, as evidenced through similar gene expression profiles or otherwise. Indeed, it has long been suggested<sup>50</sup> that ECM–cell interactions could affect hepatic gene expression. Nagaki *et al.*<sup>51</sup> proposed that ECM components regulate gene expression by activating specific hepatic transcription factors, HNF-1 and HNF-4. Since then, multiple mechanisms have been reported but, to the best of our knowledge, have not distinguished between the effects of different types of ECM proteins or combinations thereof on promoting liver-specific functions. Kimata *et al.*<sup>52</sup> more recently showed that there were differences in mRNA expression levels when cells were cultured on collagen type I, collagen type IV, laminin, or EHS gels and complex gels in a 2D culture system. Based on these findings, it would be expected that there will be some differences in liver-specific functions depending on which ECM protein(s) is conjugated to the ICC scaffold. Collagen type I was chosen in our study because of its known importance and prevalence in the hepatic microenvironment, although there is significant potential to utilize the ICC platform for further exploring the functional effects of other ECM proteins as well.

## 5. Conclusions

ECM proteins play a significant role in regulating various cell behaviors, including cell adhesion, function, and migration among others. Using facile microfabrication techniques and EDC/NHS chemistry, we combined two facets of the hepatic microenvironment, ECM presence and 3D geometry, to fabricate collagen-conjugated PEG-DA ICC scaffolds with porous topology for Huh-7.5 cell culture. Our results reveal the successful infiltration of cells into the bioactive scaffolds and the presence of collagen promoted cell-scaffold adhesion and cell–cell interaction, directing the cells into multilayer cell sheets that lined the cavity walls. In comparison to 2D cell platforms and 3D bare ICC scaffold culture, the Col I-conjugated hepatocyte culture enhanced cell proliferation, albumin secretion, CYP450 activity and up-regulated adhesion gene expression in addition to other liver-specific genes. This work shows the potential of this scaffold to be used in liver tissue engineering for the applications of tissue regeneration, xenobiotic toxicity studies, and disease study.

## Acknowledgements

The authors wish to acknowledge support from a National Research Foundation Fellowship (NRF-NRFF2011-01) and Competitive Research Programme (NRF-CRP10-2012-07).

## References

- 1 M. Müller and P. L. M. Jansen, *J. Hepatol.*, 1998, **28**, 344–354.
- 2 S. N. Bhatia, G. H. Underhill, K. S. Zaret and I. J. Fox, *Sci. Transl. Med.*, 2014, **6**, 245sr242.
- 3 K. A. Brown, *Curr. Opin. Gastroenterol.*, 2005, **21**, 331–336.
- 4 C. Chan, F. Berthiaume, B. D. Nath, A. W. Tilles, M. Toner and M. L. Yarmush, *Liver Transpl.*, 2004, **10**, 1331–1342.
- 5 M. Miyazaki, Y. Handa, M. Oda, T. Yabe, K. Miyano and J. Sato, *Exp. Cell Res.*, 1985, **159**, 176–190.
- 6 T. Croci and G. M. Williams, *Biochem. Pharmacol.*, 1985, **34**, 3029–3035.
- 7 M. H. Grant, M. A. Melvin, P. Shaw, W. T. Melvin and M. D. Burke, *FEBS Lett.*, 1985, **190**, 99–103.
- 8 L. Xia, S. Ng, R. Han, X. Tuo, G. Xiao, H. L. Leo, T. Cheng and H. Yu, *Biomaterials*, 2009, **30**, 5927–5936.
- 9 J. Dunn, M. Yarmush, H. Koebe and R. Tompkins, *FASEB J.*, 1989, **3**, 174–177.
- 10 F. Berthiaume, P. V. Moghe, M. Toner and M. L. Yarmush, *FASEB J.*, 1996, **10**, 1471–1484.
- 11 J. Dunn, R. G. Tompkins and M. L. Yarmush, *J. Cell Biol.*, 1992, **116**, 1043–1053.
- 12 J. C. Dunn, R. G. Tompkins and M. L. Yarmush, *Biotechnol. Prog.*, 1991, **7**, 237–245.
- 13 S. Zhang, L. Xia, C. H. Kang, G. Xiao, S. M. Ong, Y. C. Toh, H. L. Leo, D. van Noort, S. H. Kan and H. H. Tang, *Biomaterials*, 2008, **29**, 3993–4002.
- 14 M. Hegde, R. Jindal, A. Bhushan, S. S. Bale, W. J. McCarty, I. Golberg, O. B. Usta and M. L. Yarmush, *Lab Chip*, 2014, **14**, 2033–2039.
- 15 G. D. Tan, G. W. Toh, E. Birgersson, J. Robens, D. van Noort and H. L. Leo, *Biotechnol. Bioeng.*, 2013, **110**, 1663–1673.
- 16 C. Y. Li, K. R. Stevens, R. E. Schwartz, B. S. Alejandro, J. H. Huang and S. N. Bhatia, *Tissue Eng., Part A*, 2014, 2200–2212.
- 17 K. R. Stevens, J. S. Miller, B. L. Blakely, C. S. Chen and S. N. Bhatia, *J. Biomed. Mater. Res., Part A*, 2015, 3331–3338.
- 18 D. R. Albrecht, V. L. Tsang, R. L. Sah and S. N. Bhatia, *Lab Chip*, 2005, **5**, 111–118.
- 19 N. A. Kotov, Y. Liu, S. Wang, C. Cumming, M. Eghtedari, G. Vargas, M. Motamedi, J. Nichols and J. Cortiella, *Langmuir*, 2004, **20**, 7887–7892.
- 20 Y. Liu, S. Wang, J. W. Lee and N. A. Kotov, *Chem. Mater.*, 2005, **17**, 4918–4924.
- 21 J. Lee, M. J. Cuddihy, G. M. Cater and N. A. Kotov, *Biomaterials*, 2009, **30**, 4687–4694.
- 22 J. Lee, G. D. Lilly, R. C. Doty, P. Podsiadlo and N. A. Kotov, *Small*, 2009, **5**, 1213–1221.
- 23 Y. Zhang, S. Wang, M. Eghtedari, M. Motamedi and N. A. Kotov, *Adv. Funct. Mater.*, 2005, **15**, 725–731.
- 24 R. M. Sutherland, *Science*, 1988, **240**, 177–184.

- 25 M. H. Kim, S. K. Kumar, H. Shirahama, J. Seo, J. H. Lee, V. P. Zhdanov and N.-J. Cho, *Macromol. Biosci.*, 2015, DOI: 10.1002/mabi.201500338.
- 26 C. Frantz, K. M. Stewart and V. M. Weaver, *J. Cell Sci.*, 2010, **123**, 4195–4200.
- 27 S. Beken, K. Slaus, K. De Smet, M. Depreter, F. Roels, A. Vercruyse and V. Rogiers, *Toxicol. in Vitro*, 1999, **13**, 571–577.
- 28 R. G. Wells, *Hepatology*, 2008, **47**, 1394–1400.
- 29 D. J. Waters, K. Engberg, R. Parke-Houben, L. Hartmann, C. N. Ta, M. F. Toney and C. W. Frank, *Macromolecules*, 2010, **43**, 6861–6870.
- 30 D. L. Elbert and J. A. Hubbell, *Biomacromolecules*, 2001, **2**, 430–441.
- 31 J. Li, J. Pan, L. Zhang and Y. Yu, *Biomaterials*, 2003, **24**, 2317–2322.
- 32 C. Maslansky and G. Williams, *In Vitro Cell. Dev. Biol.: Plant*, 1982, **18**, 683–693.
- 33 S. Jeong, M. Rebeiz, P. Andolfatto, T. Werner, J. True and S. B. Carroll, *Cell*, 2008, **132**, 783–793.
- 34 K. J. Livak and T. D. Schmittgen, *Methods*, 2001, **25**, 402–408.
- 35 S. Rozen and H. Skaletsky, *Methods Mol. Biol.*, 2000, **132**, 365–386.
- 36 H. Nacer-Cherif, B. Bois-Joyeux, G. Rousseau, F. Lemaigre and J. Danan, *Biochem. J.*, 2003, **369**, 583–591.
- 37 A. Kamiya, T. Kinoshita, Y. Ito, T. Matsui, Y. Morikawa, E. Senba, K. Nakashima, T. Taga, K. Yoshida and T. Kishimoto, *EMBO J.*, 1999, **18**, 2127–2136.
- 38 G. A. Silverman, P. I. Bird, R. W. Carrell, P. B. Coughlin, P. G. Gettins, J. I. Irving, D. A. Lomas, C. J. Luke, R. W. Moyer and P. A. Pemberton, *J. Biol. Chem.*, 2001, 33293–33296.
- 39 T. Touboul, N. R. Hannan, S. Corbineau, A. Martinez, C. Martinet, S. Branchereau, S. Mainot, H. Strick-Marchand, R. Pedersen and J. Di Santo, *Hepatology*, 2010, **51**, 1754–1765.
- 40 R. C. Nordlie, J. D. Foster and A. J. Lange, *Annu. Rev. Nutr.*, 1999, **19**, 379–406.
- 41 K. Nakata, Y. TANAKA, T. Nakano, T. Adachi, H. Tanaka, T. Kaminuma and T. Ishikawa, *Drug Metab. Pharmacokinet.*, 2006, **21**, 437–457.
- 42 C. P. Martinez-Jimenez, R. Jover, M. Teresa Donato, J. V. Castell and M. Jose Gomez-Lechon, *Curr. Drug Metab.*, 2007, **8**, 185–194.
- 43 M. Takeichi, *Science*, 1991, **251**, 1451–1455.
- 44 M. C. Moh, L. H. Lee and S. Shen, *J. Hepatol.*, 2005, **42**, 833–841.
- 45 K. Anderson, L. Yin, C. Macdonald and M. H. Grant, *Toxicol. in Vitro*, 1996, **10**, 721–727.
- 46 A. L. Harris, *Nat. Rev. Cancer*, 2002, **2**, 38–47.
- 47 F. Chen, S. Gerber, V. M. Korkhov, S. Mireku, M. Bucher, K. P. Locher and R. Zenobi, *J. Am. Soc. Mass Spectrom.*, 2015, **26**, 493–498.
- 48 Y. Sakai, M. Koike, H. Hasegawa, K. Yamanouchi, A. Soyama, M. Takatsuki, T. Kuroki, K. Ohashi, T. Okano and S. Eguchi, *PLoS One*, 2013, **8**, e70970.
- 49 L. Fu, S. S. Dong, Y. W. Xie, L. S. Tai, L. Chen, K. L. Kong, K. Man, D. Xie, Y. Li and Y. Cheng, *Hepatology*, 2010, **51**, 1624–1634.
- 50 A. Ben-Ze'ev, G. S. Robinson, N. Bucher and S. R. Farmer, *Proc. Natl. Acad. Sci. U. S. A.*, 1988, **85**, 2161–2165.
- 51 M. Nagaki, Y. Shidoji, Y. Yamada, A. Sugiyama, M. Tanaka, T. Akaike, H. Ohnishi, H. Moriwaki and Y. Muto, *Biochem. Biophys. Res. Commun.*, 1995, **210**, 38–43.
- 52 T. Kimata, M. Nagaki, T. Ogiso, T. Naiki, T. Kato and H. Moriwaki, *Hepatology*, 2006, **44**, 140–151.